Production of Fluorine-Containing Molecular Species in Plasma-Generated Atomic F Flows

G. J. Stueber,[†] S. A. Clarke,[†] E. R. Bernstein,*,[†] S. Raoux,[‡] P. Porshnev,[‡] and T. Tanaka[‡]

Department of Chemistry, Colorado State University, Fort Collins, Colorado 80523-1872, and Applied Materials, Inc., 3050 Bowers Avenue, Santa Clara, California 95054

Received: March 18, 2003; In Final Form: June 17, 2003

The fluorine atomic radical reactions to form molecular fluorine and hydrogen fluoride are examined by time-of-flight mass spectroscopy (TOFMS) and kinetically modeled for various reaction orders. Fluorine radicals are generated from NF_3 or F_2 in microwave-generated and low-frequency (LF)-generated plasmas and are passed through flow tubes under various flow, pressure, and dilution conditions. In general, the concentrations of the mass spectroscopically measured products F, F_2, and HF do not depend on the specific wall material (e.g., Teflon, stainless steel, Al, Ni, Al_2O_3, SiO_2); the only variations of [F]/[F_2]/[HF] ratios with wall material are found at pressures below 1 Torr. The most significant changes in these ratios are observed upon varying flow rates and pressures. Specifically, the F relative concentration decreases from ∼80% to ∼20%, and the F_2 relative concentration increases from ∼20% to ∼80%, as the pressure is varied over the range 0.5−10 Torr. In all cases, the HF concentration is found to decrease as the pressure increases. Data suggest that the composition of the tube surface material does not contribute significantly to the generation of F_2; however, since the wall surface carries adsorbed hydrogen sources such as H, H_2O, H_2, and OH, it becomes important in the generation of HF. A simple kinetic analysis of the experimental data suggests a combined two-reaction mechanism for F_2 and HF generation: (1) a pseudo-second-order volume reaction (k_v) to generate F_2, and (2) a zero- or first-order wall reaction (k_w) to generate HF. Thus, both surface and volume reactions contribute to the overall F atom loss mechanism in the gas flow from the plasma source. The model fits our data best for a k_v/k_w ratio of about 75. The reaction order for the loss of F atom is found to be 1.68, while the reaction order for the formation of F_2 is found to be ∼2.

I. Introduction

Fluorine-containing plasmas are used extensively in the semiconductor industry for etching[1−12] and chemical vapor deposition (CVD) chamber cleaning purposes.[13−16] Our work is aimed toward increasing knowledge of the basic chemistry involving the transport of fluorine atoms[17−30] (the assumed cleaning species) derived from fluorine-containing plasmas in order to manipulate such plasmas to maximize chamber cleaning and etching efficiency, and to minimize hazardous waste products.[31−36] To gain this understanding, we are exploring a broad range of operating parameter space with regard to plasma feed gas composition, flow tube material, flow rates, reactive gas pressure, and diluent gas. We utilize time-of-flight mass spectroscopy (TOFMS) and laser-induced fluorescence detection to measure the relative amounts of different, chemically important species and their energetic states. These studies explore a range of operating parameters that are closely related to those employed for chamber cleaning (and wafer etching), and they establish the extremes of the ranges over which interesting and meaningful results can be monitored. Parameters that are studied include wall materials (such as aluminum, quartz, aluminum oxide, Teflon, nickel, and others), pressures, and flow rates, and their interdependence. Such studies are undertaken using different plasma sources (microwave and inductively coupled low frequency, LF). The majority of the data reported here is for an LF source.

The results thus obtained are analyzed to determine the relative importance of the different experimental parameters in the molecular fluorine formation reaction.[37,38] They are also analyzed to determine the kinetics and mechanisms of the F_2 and HF formation reactions.[39−41] The results of the kinetic and mechanistic analysis of these data are discussed. The data collected are analyzed by two elementary reaction mechanisms involving a pseudo-second-order gas-phase reaction and a first-order wall reaction.

II. Experimental Procedures

The plasma is generated by an Advanced Energy Rapid F instrument (typically 2−6 kW at 400 kHz of LF power) for the majority of the results reported here, with some comparisons to the Applied Materials DCVD Centura μClean microwave source (∼1.2 kW microwave power). The experimental setup used in these studies is shown in Figure 1. A 12-in.-long (1.35 in. i.d.) tube (indicated by W in Figure 1) is mounted to the source exit. This is the main wall material test section: tube wall materials are varied to include aluminum, anodized aluminum, stainless steel, quartz, monel, nickel, Teflon, or copper. After this tube is a 5-in.-long tube that carries the Baratron pressure sensor (G). This 5-in. section can be either stainless steel (when the main test tube is stainless) or aluminum (all other cases). Pressures are adjusted between 100 mTorr and 10 Torr by a Teflon butterfly valve (BV) mounted after the

* To whom correspondence should be addressed.
[†] Colorado State University.
[‡] Applied Materials, Inc.

10.1021/jp030339i CCC: $25.00 © 2003 American Chemical Society
Published on Web 08/30/2003

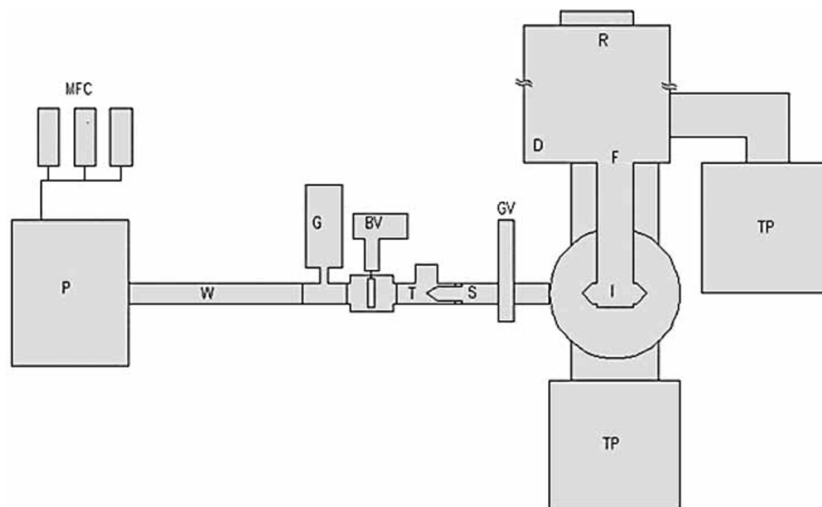

Figure 1. Experimental setup: P, plasma source; W, wall material test section; BV, butterfly or throttle valve used to control pressure; I, ionization region of TOFMS; MFC, mass flow controller (gas inlet manifold); G, Baratron pressure gauge; T, tee section; S, skimmer; GV, gate valves; F, TOFMS flight tube; D, detector; R, reflectron assembly; and TP, turbomolecular pumps. See text for detailed explanation of the apparatus.

Baratron gauge and before a dry pump. Immediately after this throttle valve is an aluminum tee (T) with the sampling skimmer (S) for the mass spectrometer mounted in the flow about 2 in. downstream from the throttle valve (BV) exit.

A small fraction of the gas flow passes through a 0.5-mm skimmer (S) into the main chamber of the TOFMS. This first TOFMS main chamber is held at $\sim 10^{-5}$ Torr. The gas flow enters, through a 4-mm skimmer, the ion source of a Wiley–McLaren-type TOFMS[42,43] at $<3 \times 10^{-7}$ Torr. In the TOF ion source, the neutrals are ionized by an ArF (193 nm) excimer laser beam or by photoelectrons ejected from a stainless steel target mounted at the exit port of the ionization chamber (I). Under our conditions, one ion is created out of about 1000 neutrals. Data are recorded with a focused ionization laser beam at laser fluences up to 250 mJ/cm^2. Under multiphoton ionization conditions such as those employed in this work, species may fragment upon ionization. To ascertain the degree of NF_3 and F_2 fragmentation, we collect mass spectral distributions and signal intensities under plasma *on* and *off* conditions.

The ions so produced are extracted perpendicularly to the flow axis by a 1.2-kV electric field and enter a 1.5-m-long flight tube (F), where they are separated in time according to their mass. At the end of the flight tube, the ions are detected by an 18-mm Galileo multichannel plate detector if the spectrometer is used in *linear* mode. The MS also has the capability of operating in a *reflectron* mode. In this case, the ions pass through the field-free region onto the ion mirror reflection stage (R), from which they are repelled and accelerated toward the detection device, an ETP AF850H electron multiplier or a 40-mm Galileo multichannel plate (D). In the corrosive $F/HF/F_2$ environment, the more robust ETP detector is preferred, but both detectors have a very limited lifetime, on the order of a few months, in this environment. The signal from the detector is passed to a Tektronix RTD 720A transient digitizer that samples the detector output voltage at 4 ns/bin and transfers the data to an A/D converter and finally to a Gateway G6-180 personal computer for manipulation and storage.

The flow tubes and system are cleaned and passivated with a F plasma for several minutes before data are collected for a particular flow rate or pressure. Data are collected at various pressures and flows, varying the conditions in different orders in different data sets to eliminate systematic errors from

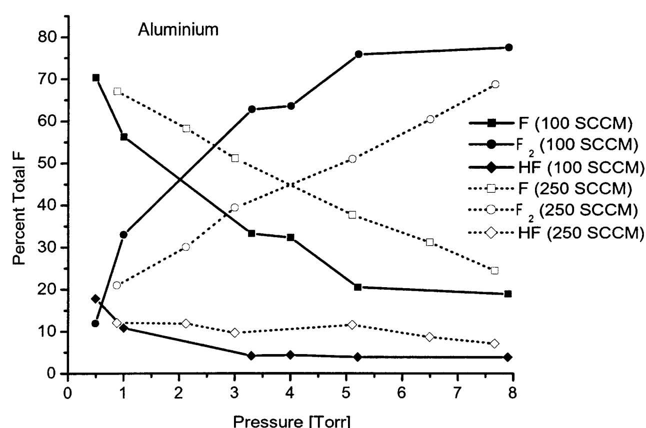

Figure 2. Percentage of F atoms in $F/HF/F_2$: aluminum walls. A plot of the percentage of total F atoms found in each of the three ($F/HF/F_2$) possible F-containing species for a 12-in. test section of aluminum wall versus total pressure.

changing system conditions. Data from sets taken by varying the pressure from high to low are the same as data taken by varying the pressure from low to high. Ratios of F-containing species are consistent from run to run, and with both types of detectors. Mass flow calibration runs (based on Ar, N_2, and total F concentrations) are performed for the data sets and are accurate and reproducible to $\pm 10\%$.

III. Results and Discussion

In our experimental arrangement, the effluent F stream flows through tubes made of eight different materials (aluminum, anodized aluminum, aluminum oxide, quartz, Teflon, nickel, monel, and stainless steel). The materials chosen present a wide array of materials that could possibly be used in industrial settings. The data for aluminum represent the base system to which we will compare all other findings. Figure 2 shows the pressure dependence of the observed percentages of F species for flows of 100 and 250 sccm (standard cubic centimeters per minute) for aluminum wall materials. Higher flows, up to 1000 sccm, give results very similar to these.

As can be seen in Figure 2, the percentage of the fluorine found as F atoms decreases with increasing pressure, the

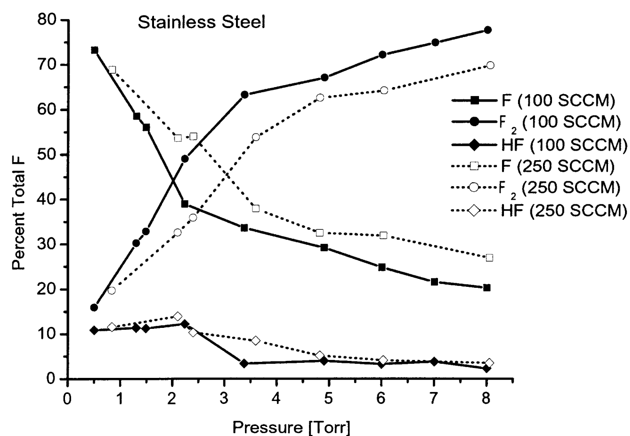

Figure 3. Percentage of F atoms in $F/HF/F_2$: stainless steel walls. A plot of the percentage of total F atoms found in each of the three ($F/HF/F_2$) possible F-containing species for a 12-in. test section of stainless steel wall versus total pressure.

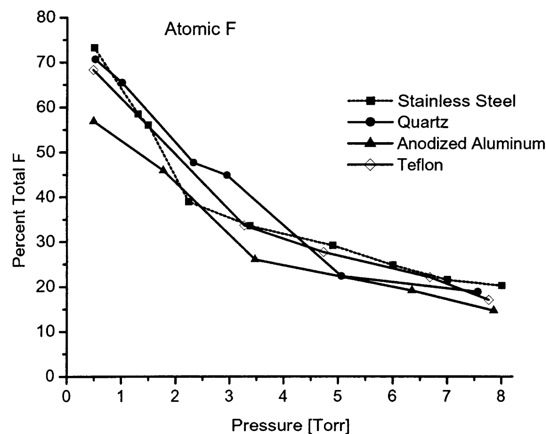

Figure 4. F atom percentage versus pressure for different wall materials. A plot of the percentage of total F atoms in plasma found as atomic F vs total pressure for different wall materials, as indicated in the figure.

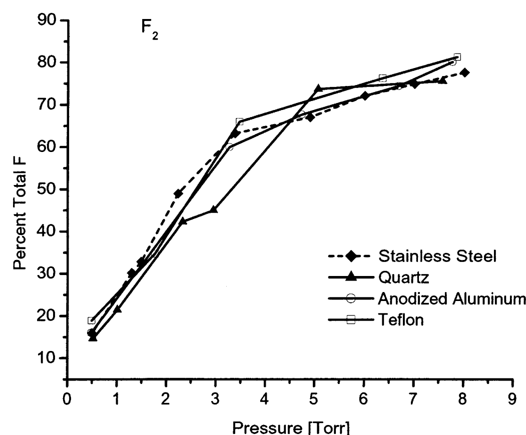

Figure 5. F_2 molecule percentage versus pressure for different wall materials. A plot of the percentage of total F atoms in plasma found as molecular F_2 vs total pressure for different wall materials, as indicated in the figure.

percentage of fluorine found as F_2 molecules increases steeply with increasing pressure, and the percentage of fluorine detected as HF is small and also decreases with increasing pressure. The appearance of HF is the result of contamination with H-containing species (water, hydrogen) adsorbed on the tube walls or held within the bulk material and subsequent reaction with F. Commercial reactors apparently generate less HF than found in these laboratory studies.

When working with the other very different tube materials, we note particularly the same increasing F_2 percentage and decreasing F percentage with increasing total pressure; for instance, see Figure 3 with data from stainless steel wall material. Monel, nickel, and Teflon are also employed as wall materials in these studies. Monel and nickel are known to passivate in the presence of $F/HF/F_2$, even at temperatures in excess of 1000 °C, and so-called end-capped PFA-type Teflon is believed to be the most inert type of Teflon. Despite the very different surfaces that monel, nickel, and Teflon present compared to other wall materials employed, the trends in F and F_2 percentages are fundamentally the same as those reported for aluminum and stainless steel. The measured F_2 percentage is similarly related largely only to total pressure, and the measured F percentage is inversely related largely only to total pressure, as seen in all previous experiments. In general, concentration differences for F and F_2 can be dependent on walls and flows, but only at very low pressures. These differences can matter ($\pm$20%) but need to be more thoroughly explored from <100 mTorr to ~1 Torr. The variation of the %[F] values from run to run is probably $\pm$10%. All of the plots are very similar, despite very different wall materials. One would expect that reactive surfaces such as quartz would offer an exceedingly different surface to the wall recombination process than Teflon, yet the results are fundamentally the same. The pressures (1−10 Torr) and the flow rates (100−1000 sccm) make all the difference, and the wall material is essentially irrelevant over this range of pressures and flows. Only at the lowest pressures (generally less than 1 Torr) are any significant differences between the wall materials observed. Figure 4 summarizes the %[F] vs pressure findings for several materials, and Figure 5 presents the %[F_2] vs pressure finding for the same materials.

On the basis of these observations, we postulate that a surface reaction may be responsible for HF generation and that F reaction to form F_2 occurs mostly in the gas phase.

IV. Kinetic and Mechanistic Analysis of MS Data

A. Procedures and Equations. In a conventional flow kinetics experimental system, a constant velocity of material flows through a mixing tube, and measurements of the concentrations of reactant and products are made at different points in the flow tube. Concentrations of reactants and products are obtained as a function of time by measuring these concentrations at different distances from the point of mixing or generation of the reactants. Plots of concentration vs time can be made, and reaction rate constants can be determined from them in the usual textbook manner.[44−46]

An alternative method to vary the time axis for the reaction is to change the velocity or residence time of the material being studied, while keeping a constant sampling distance or tube length. In this case, the "time" axis is actually the flow velocity axis, and the reactant velocity (residence time) is varied by controlling flow and pressure. This latter method is much better suited to the physical requirements of our system and the nature of the experiments pursued.

The first step in the data analysis for a fixed sampling point position study is to find a relationship between velocity (and hence time since start of reaction at a fixed point) and the pressure and flow rate. Using the ideal gas law and the definition of velocity as a starting point, one can derive the

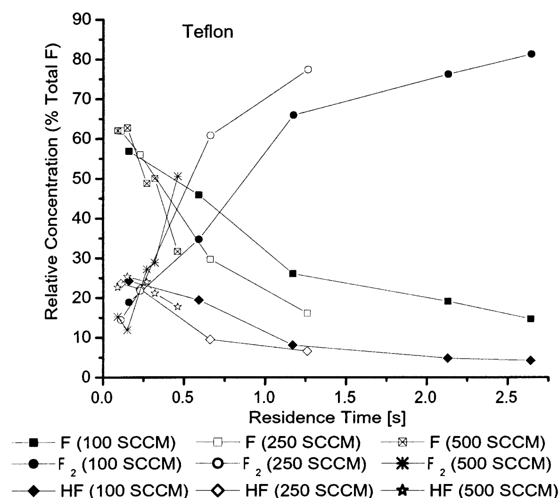

Figure 6. Relative concentration vs residence time: Teflon. A plot of relative concentration (F/F_0, HF/F_0, F_2/F_0) vs residence time in wall material test section for Teflon-lined aluminum tube.

following relationship between residence time and pressure and flow:

$$\tau(\mathrm{s}) = \left[\frac{1}{F\left(\frac{\mathrm{scc}}{\mathrm{min}}\right)}\right][P(\mathrm{Torr})] \times \left\{\frac{[A(\mathrm{cm}^2)][L(\mathrm{cm})]}{[T(\mathrm{K})]}\right\}\left\{\frac{[298(\mathrm{K})[60(\mathrm{s})]}{[760(\mathrm{Torr})]}\right\}\left\{\frac{[1(\mathrm{scc})]}{[1(\mathrm{cm}^3)][1(\mathrm{min})]}\right\}$$

$$or \qquad (1)$$

$$\tau = \{P\}\left\{\frac{1}{F}\right\}\left\{\frac{AL}{T}\right\}\{23.53\}$$

in which τ is residence time, F is mass flow (in sccm), A and L are cross-section area and length of the flow tube, and T is temperature. Using this result, the residence time of the reactive species in the wall material test section can be calculated. These results are given in the following section.

The basic data presentation for kinetics information is the plot given in Figure 6, namely relative concentration vs residence time. To account for the initial concentration variation with different flow rates, we plot $[F]_r = [F]/[F]_o$ (or $[HF]/[F]_o$, $[F_2]/[F]_o$), the relative (or normalized) concentration versus residence time.

To get from those plots to a mechanism, one postulates a mechanism, computes $[X]_r$ vs residence time, and compares the results to the experimental data. For example, one could postulate that the reaction is a simple first-order reaction in F. To test that possibility, one would plot ln [F] vs time. If the reaction is first order, that plot will produce a straight line with slope k, the rate constant for the reaction. This is the standard procedure outlined in nearly any kinetics textbook for a static system.[44−46]

The procedure is more complicated for a flow system such as that used in our experiments, but the same basic procedure can be applied—a mechanism is postulated, and its kinetics results are compared to the experimental results. Several basic mechanisms are reasonable for the possible reactions that might occur. Below we compare the rate predictions for these mechanisms with those derived for the data from the experimental studies.

B. Single Reaction Mechanisms. Only a handful of elementary reactions are commonly observed, namely zero order, first order, second order, pseudo-second order, and third order. The simplest mechanism for the F_2 formation reaction would be one single elementary step. We start by analyzing the data relative to these elementary steps.

1. Second Order. The simplest elementary reaction mechanism that would make sense for the F_2 formation reaction is a second-order reaction, such as

$$F + F \xrightarrow[k_s]{} F_2 \qquad (2)$$

The rate equation for this reaction is

$$R \equiv \frac{d[F]}{dt} = -2k_s[F]^2 \qquad (3)$$

By integrating the above equation, the integrated rate equation is

$$\frac{1}{[F]} = -2k_s t + \frac{1}{[F]_o} \qquad (4)$$

Plotting $[F]^{-1}$ vs time should yield a straight line of slope $2k_s$, from which the rate constant k_s can easily be determined; however, the experimental data do not produce a straight line when plotted in this manner, and thus, a single second-order reaction is not an acceptable mechanism for the formation of F_2 in this experiment.

2. Pseudo-Second Order. A mechanism for a third-order/pseudo-second-order reaction for a recombination reaction is

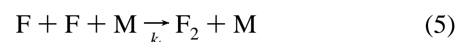

$$F + F + M \xrightarrow[k_t]{} F_2 + M \qquad (5)$$

in which M is any third body to remove the excess collision energy and k_t is the third-order reaction rate constant. The rate for this reaction is written as

$$R \equiv \frac{d[F]}{dt} = -2k_t[F]^2[M] \qquad (6)$$

In cases such as recombination, for which [M] is constant during the reaction, this equation can be rewritten as

$$R \equiv \frac{d[F]}{dt} = -2k_{ps}[F]^2 \qquad (7)$$

in which k_{ps} is the pseudo-second-order reaction rate constant. The reaction (5) is called "pseudo-second order" since the measured rate constant, k_{ps}, is not a real rate constant (which must be a constant), but rather it is dependent on the total concentration (or total pressure in our case). By integrating the above equation, the integrated rate equation is obtained:

$$\frac{1}{[F]} = -2k_{ps}t + \frac{1}{[F]_o} \qquad (8)$$

Plots of $[F]^{-1}$ vs time should yield a series of lines (one for each [M]), and the slope of each of these lines is $2k_{ps}$ for that [M]. The true third-order rate constant is then found from a plot of k_{ps} vs [M].

The flow system that we have adds an extra level of complexity to this analysis. Since the concentration of third bodies ([M]) and time (t) are both dependent on pressure, this dependence must be included in the integration. Thus,

$$\int \frac{\mathrm{d}[\mathrm{F}]}{[\mathrm{F}]^2} = \int -2k_t[\mathrm{M}]\,\mathrm{d}t$$

$$\frac{1}{[\mathrm{F}]} - \frac{1}{[\mathrm{F}]_o} = -2k_t\left\{\frac{P}{RT}\right\}\left\{P\frac{1}{F}\left(\frac{LA}{T}\right)\left(\frac{760 \times 60}{298}\right)\right\} \tag{9}$$

$$\frac{1}{[\mathrm{F}]} = -2k_{ps}P^2 + \frac{1}{[\mathrm{F}]_o}$$

in which k_{ps} is k_t (the true three-body rate constant) divided by the flow and a series of constants (note that in eq 9, [F] is the concentration of F atoms, and $1/F$ is the inverse of the NF_3 flow, in sccm). Thus, a plot of the inverse of concentration vs total pressure squared will produce a series of lines with slope $2k_{ps}$. From these k_{ps} values, the true three-body rate constant can be calculated.

To be able to observe this dependence, all the data for F atom concentration based on different wall materials are analyzed together in a plot of inverse F atom concentration vs (pressure)^2. This graph has some of the characteristics of the theoretical plot. Data for different flow rates are grouped and have different slopes. The low-flow data are generally above the high-flow data; however, the pseudo-second-order model does not explain all the observations, either. Noticeably missing are any explanation of the HF concentration and an explanation of the low-pressure region. In the low-pressure region, pseudo-second-order assumptions break down, and the reaction looks more like third order.

3. Zero Order. Zero-order reaction kinetics are possible in several ways. First, surface reactions tend to have zero-order kinetics. Also, saturated systems have zero-order kinetics. In zero-order kinetic reactions, the concentrations of reactants and products at a given time are related only to time, not to the concentrations at that time as well, as they are in all other orders. A plot of concentration vs time should give a straight horizontal line. This is not what is observed in the present experiments.

C. Two Reaction Mechanisms. The above zero-, first-, second-, and third-order elementary reactions do not generate satisfactory rate equations for the observed $[\mathrm{F}]/[\mathrm{F}_2]/[\mathrm{HF}]$ vs time dependences, and thus a more complex mechanism must be responsible for the experimental behavior. Using the following equation,

$$\frac{1}{[\mathrm{A}]^{n-1}} = -(n-1)kt + \frac{1}{[\mathrm{A}]_o^{\,n-1}} \tag{10}$$

the overall order n for a rate expression due to a complex mechanism can be determined. One plots the inverse of concentration raised to a particular power vs time, and then finds which value of n (reaction order) gives the best fit to the experimental data. We find that $n = 1.68$ gives the best fit to the F atom loss data, and $n \approx 2$ gives the best fit to the F_2 molecule formation data.

1. Pseudo-Second-Order Gas-Phase and Zero-Order Wall Reactions. Non-integer reaction orders are possible for more complicated mechanisms if more than one elementary reaction is involved. A two-reaction mechanism, with a pseudo-second-order component and a zero-order component, can be postulated. One possibility is the following two-reaction mechanism scheme:

$$\mathrm{F} + \mathrm{F} + \mathrm{M} \xrightarrow[k_v]{} \mathrm{F}_2 + \mathrm{M}\ (\text{volume}) \qquad \{\text{pseudo-second order}\}$$

$$\mathrm{F} + \mathrm{H} \xrightarrow[k_w]{} \mathrm{HF}\ (\text{wall}) \qquad \{\text{ zero order}\}$$

This mechanism makes sense relative to the general trends of the data. The production of HF must come from the walls, as walls are the only reasonable source of hydrogen in the system. The major reaction for the loss of [F] is conjectured to be the gas-phase reaction, due to the only minor dependence (and only at low pressure) of the reaction on wall material. Note, too, that the F−F bond is ~35 kcal/mol and the H−F bond is ~150 kcal/mol.

In much the same way as with the single elementary reaction, the rate equations for the species in the reaction can be employed, and an integrated rate equation can be found. Thus, Equations 11−13 are integrated to get the integrated rate laws.

$$\frac{\mathrm{d}[\mathrm{F}]}{\mathrm{d}t} = -2k_v[\mathrm{M}][\mathrm{F}]^2 - k_w \tag{11}$$

$$\frac{\mathrm{d}[\mathrm{F}_2]}{\mathrm{d}t} = k_v[\mathrm{M}][\mathrm{F}]^2 \tag{12}$$

$$\frac{\mathrm{d}[\mathrm{HF}]}{\mathrm{d}t} = k_w \tag{13}$$

These are not simple solutions:

$$[\mathrm{F}] = -\frac{1}{2} \times \frac{\tan\left(t\sqrt{2}\sqrt{k_w k_v[\mathrm{M}]} - \arctan\left(\frac{[\mathrm{F}]_o k_v[\mathrm{M}]\sqrt{2}}{\sqrt{k_w k_v[\mathrm{M}]}}\right)\right)\sqrt{2}\sqrt{k_w k_v[\mathrm{M}]}}{k_v[\mathrm{M}]} \tag{14}$$

$$[\mathrm{F}_2] = \int_0^t \frac{1}{2}\frac{\left(\tan(u\sqrt{2}\sqrt{k_w k_v[\mathrm{M}]}) - \frac{[\mathrm{F}]_o k_v[\mathrm{M}]\sqrt{2}}{\sqrt{k_w k_v[\mathrm{M}]}}\right)^2 k_w}{\left(1 + \frac{\tan(u\sqrt{2}\sqrt{k_w k_v[\mathrm{M}]})[\mathrm{F}]_o k_v[\mathrm{M}]\sqrt{2}}{\sqrt{k_w k_v[\mathrm{M}]}}\right)^2}\,\mathrm{d}u \tag{15}$$

$$[\mathrm{HF}] = k_w t \tag{16}$$

Using these equations, plots of the relative concentrations of all three species versus time (see Figure 7) can be generated. These plots more closely match the actual data than any of the individual elementary reactions. The general shapes of the curves are correct (especially the $[\mathrm{F}_2]$ and [F] curves), and at least a rough fit to the [HF] concentration vs time can be estimated, especially at longer times.

We can learn about the two reactions' rate constants as well. The ratio of k_v (true third-order rate constant, units of cm^6 molecule^{-2} s^{-1}) to k_w (zero-order rate constant, units of cm^{-3} molecule s^{-1}) must be in the range of 50−100. A ratio of 1 does not produce a crossing point for the [F] and $[\mathrm{F}_2]$ behavior in the time frame of the experimental data, and does not reproduce the data well. Similarly, a ratio of 100 or more does not produce HF concentrations that approach the levels in the data. The best fit comes from a ratio of $k_v/k_w \approx 75$.

2. Pseudo-Second-Order Gas-Phase and First-Order Wall Reactions. Other combinations of two reactions can also be tried. A pseudo-second-order volume reaction and a first-order surface reaction can be postulated. One possibility is the following two-reaction mechanism scheme:

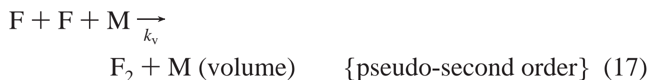

$$\mathrm{F} + \mathrm{F} + \mathrm{M} \xrightarrow[k_v]{} \mathrm{F_2} + \mathrm{M}\ \text{(volume)} \qquad \text{\{pseudo-second order\}} \tag{17}$$

$$\mathrm{F} + \mathrm{H} \xrightarrow[k_w]{} \mathrm{HF}\ \text{(wall)} \qquad \text{\{first order\}} \tag{18}$$

In much the same way as with the pseudo-second-order/zero-order mechanism, the rate equations for the species in the reaction can be employed,

$$\frac{d[\mathrm{F}]}{dt} = -2k_v[\mathrm{M}][\mathrm{F}]^2 - k_w[\mathrm{F}] \tag{19}$$

$$\frac{d[\mathrm{F_2}]}{dt} = k_v[\mathrm{M}][\mathrm{F}]^2 \tag{20}$$

$$\frac{d[\mathrm{HF}]}{dt} = k_w[\mathrm{F}] \tag{21}$$

and an integrated rate equation can be found:

$$[\mathrm{F}] = \frac{k_w}{-2k_v[\mathrm{M}] + \frac{k_w}{[\mathrm{F}]_o} e^{k_w t} + 2k_v[\mathrm{M}] e^{k_w t}} \tag{22}$$

$$[\mathrm{F_2}] = \frac{1}{2}[\mathrm{F}]_o + \frac{1}{4}\left\{\frac{{k_w}^2 t}{k_v[\mathrm{M}]}\right\} - \left\{\frac{{k_w}^2 t \ln\left(\frac{2k_v[\mathrm{F}]_o[\mathrm{M}]}{k_w}(1 - e^{k_w t})\right)}{k_v[\mathrm{M}]}\right\} - \frac{1}{2}\left\{\frac{k_w}{-2k_v[\mathrm{M}] + \frac{k_w}{[\mathrm{F}]_o} e^{k_w t} + 2k_v[\mathrm{M}] e^{k_w t}}\right\} \tag{23}$$

$$[\mathrm{HF}] = \frac{1}{2}\left\{\frac{{k_w}^2 t \ln\left(\frac{2k_v[\mathrm{F}]_o[\mathrm{M}]}{k_w}(1 - e^{k_w t})\right)}{k_v[\mathrm{M}]}\right\} - \frac{1}{2}\left\{\frac{{k_w}^2 t}{k_v[\mathrm{M}]}\right\} \tag{24}$$

Using these equations, we can again generate plots of the relative concentrations of all three species versus time (see Figure 8). The general shapes of the curves are again correct (especially the $[F_2]$ and [F] curves), and a rough fit to the [HF] concentration can also be obtained, especially at longer times.

We can learn about the two reactions' rate constants, as well. The ratio of k_v (true third-order volume rate constant, units cm^6 molecule^{-2} s^{-1}) to k_w (first-order wall rate constant, units s^{-1}) must be in the range of 35−75. A ratio of 1 does not produce a crossing point for [F] and $[F_2]$ in the time frame of the experimental data, and does not reproduce the data well. Similarly, a ratio of 75 or more does not produce HF concentrations that approach the levels we typically see in the data. The best fit to the data comes from a ratio of $k_v/k_w \approx 50$.

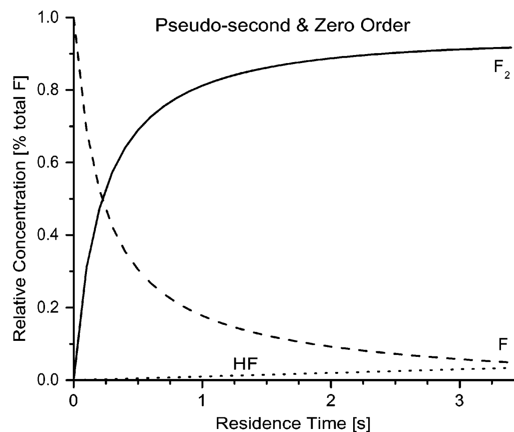

Figure 7. Relative concentration vs residence time: theoretical plot for pseudo-second-order/zero-order reaction. A theoretical plot of relative concentration (F/F_0, HF/F_0, F_2/F_0) vs residence time for a system with a pseudo-second-order volume F_2 formation reaction and a zero-order wall HF formation reaction. The ratio of k_v (true third-order rate constant) to k_w (zero-order rate constant) is 75.

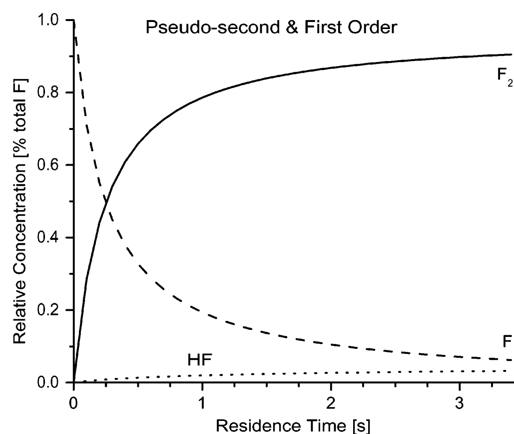

Figure 8. Relative concentration vs residence time: theoretical plot for pseudo-second-order/first-order reaction. A theoretical plot of relative concentration (F/F_0, HF/F_0, F_2/F_0) vs residence time for a system with a pseudo-second-order volume F_2 formation reaction and a first-order wall HF formation reaction. The ratio of k_w (true third-order rate constant) to k_w (first-order rate constant) is 50.

3. Other Multi-Reaction Mechanisms. An F_2 wall elementary reaction component can also be added to these reaction sets to give a three-reaction mechanism. This augmented reaction set would further complicate the mathematics and the mechanism, but would not add much insight to the overall process because only total F_2 is measured. This additional complication, while perhaps a part of the general reaction mechanism, is not demanded by the present data. Nonetheless, an F_2 wall reaction that competes with the HF wall reaction might explain the differences between the theoretical [HF] predictions and the experimental [HF] results.

Combining all the information from the kinetics studies and analysis with the information from the mass spectroscopy concentration studies allows us to make some general observations.

(1) Kinetics analysis of the mass spectroscopy data shows that surface material is not a controlling factor for the generation of HF and F_2 under the conditions employed.

(2) The loss of F atoms shows kinetics results that indicate a reaction order (order = 1.68) that is consistent with a combination of surface and volume reactions.

(3) Production of F_2 has an overall order that is close to 2.0, suggesting that the generation of F_2 is mostly through a gas-phase reaction (pseudo-second order).

(4) Data for the production of HF show a surface-independent, relatively constant level of HF, which is consistent with a surface reaction (zero or first order) that is not material dependent, but is related to the adsorbed/absorbed hydrogen in many forms (OH, H_2, H_2O, ...) present on all surfaces, and in all bulk materials, to some extent.

These four observations can be reconciled in three ways. First, a surface reaction is a major recombination pathway, but the reaction is independent of surface material and, unlike most surface reactions, is second order. Second, a surface reaction is the major recombination pathway, but the reaction is saturated for all surfaces at the typical pressures and residence times used in our experiments. We will discuss possible further experiments in the next section that could distinguish between these two possibilities. The third possibility is that the major pathway for the loss of F atoms from the gas flow is actually composed of several different elementary mechanisms of different reaction orders that are of varying importance at different pressures, making analysis of the overall mechanism difficult to interpret from a general data set. We believe that the observed data are best treated under the latter possibility. Thus, wall reactions for at least HF generation and volume reactions for F_2 generation are major elementary reactions contributing to the observed [F], [HF], and [F_2] components of the flow. Given the above possibility, the ratio of the rate constants for the third-order gas-phase reaction for F_2 generation and the zero- or first-order surface generation of HF is $k_v/k_w \approx 75$ for the zero-order wall scheme and $k_v/k_w \approx 50$ for the first-order wall scheme.

D. Comparison to Other Published Data. The recombination of F atoms derived from F_2 feed gas to re-form F_2 has been previously studied, but no other studies have been published using NF_3 feed gas. The F_2 feed gas studies give results fundamentally in agreement with our NF_3 feed gas studies, despite some differences in experimental procedures. The F_2 feed gas studies were done with different buffer gases to take away the excess energy (Ar, He, etc), with much lower F atom mole fractions (1−25%), and at much higher pressures (1−500 Torr). In addition, most of the earlier work used chemiluminescent titration of F atoms with chlorine. Such measurements were found to be susceptible to error due to the complexity of halogen atom recombination processes.[52]

A comprehensive wall recombination study at low F atom pressures (<0.2 Torr) and short residence times (<0.05 s) was published by Nordine and LeGrange.[53] Here, the use of aluminum vs alumina yielded similar F atom loss probabilities if the materials were left untreated. This similarity is due to the formation of a passivating aluminum fluoride surface layer on both materials. When cleaned with dilute HF, the neat aluminum surface contributed to an order of magnitude higher consumption of F atoms.

The present F_2 and NF_3 feed gas study conditions are chosen in order to investigate better the pseudo-second-order kinetics of the system and to match the conditions typically employed by the semiconductor industry. But, despite these differences, the same major conclusions can be seen in both sets of experiments.

The reported F_2 feed gas studies[47−51] model the F atom recombination as a combination of pseudo-second-order volume reaction ($F + F + M \rightarrow M + F_2$) and first-order wall reaction ($F + F \rightarrow F_2$). The first-order wall recombination reaction is found to be negligible relative to the pseudo-second-order volume recombination, especially at low (<10 Torr) pressures. The volume rate constant (k_v) is on the order of 10^{-34} cm^6 molecule^{-2} s^{-1} over a pressure range from about 10 Torr to several hundred Torr total pressure.

TABLE 1: Pseudo-Second-Order Volume Reaction Rate Constants for $F + F + M \rightarrow M + F_2$

rate constant (cm^6 molecule^{-2} s^{-1})	collision gas M	temp (K)	ref(s)
7×10^{-33}	He	300−500	54
4.1×10^{-35}	He	300	55
$(6 \pm 1) \times 10^{-34}$	He	300	48
$(8 \pm 0.6) \times 10^{-35}$	Ar	300	60
$(3.7 \pm 1.1) \times 10^{-35}$	Ar	300	56
$(4.7 \pm 1.2) \times 10^{-34}$	F_2	300	47
8×10^{-34}	N_2	300	60[a]
10^{-34}			57−59[b]

[a] Estimated on the basis of preliminary data. [b] Calculated.

The present NF_3 feed gas studies find very similar conclusions. These data are modeled with a pseudo-second-order volume F_2 formation reaction ($F + F + M \rightarrow M + F_2$) and a first-order HF formation reaction ($H + F \rightarrow HF$). As with the F_2 feed gas data, the NF_3 feed gas data find a first-order F_2 wall formation reaction ($F + F \rightarrow F_2$) to be negligible. The NF_3 feed gas data also give rate constants within the range of 10^{-34} cm^6 molecule^{-2} s^{-1}. For example, the data for Teflon liners (comparable to a Teflon-coated system reported in ref 60; see Table 1) produce a true third-order rate constant, k_v, of magnitude 10^{-33}−10^{-34} cm^6 molecule^{-2} s^{-1} over a pressure range from 0.5 to 10 Torr.

V. Conclusion

The reaction pathways for fluorine radicals, generated from NF_3 or F_2 in microwave and RF plasmas, are investigated by TOFMS. The two products identified are F_2 and HF. The concentrations of the mass spectroscopically measured effluent species F, F_2, and HF do not, in general, depend on wall material in the range $1 \leq P \leq 10$ Torr; the only variations of [F]/[F_2]/[HF] ratios with respect to wall material are found under low-pressure conditions (below 1 Torr). The most significant changes in gas concentration are observed as a function of flow rate and total pressure. Specifically, the F relative concentration decreases from 80% to 20%, and the F_2 relative concentration increases from 20% to 80%, upon increasing the pressure from 0.5 to 10 Torr. In all cases, the HF relative concentration is found to decrease with increasing pressure, although the overall changes are small. Since the concentration of F radical does not depend on the nature of the transport tubes, we conclude that the $F + F \rightarrow F_2$ reaction predominantly occurs in the gas phase. Conversely, the uptake of surface-bound H by F radicals leads to HF.

Since both surface and volume reactions contribute to the overall loss mechanism for F radicals, we fit our experimental data to a set of kinetic equations to obtain the overall reaction order. F reaction to form F_2 is best modeled as a third-order/pseudo-second-order reaction,

$$F + F + M \xrightarrow[k_v]{} F_2 + M$$

in which M is any third body to remove the excess energy and k_v is the third-order reaction rate constant. HF generation on the surface can be modeled as either a zero-order or first-order reaction with rate constant k_w.

The model fits our data best for a k_v/k_w ratio of about 75 (for a zero-order wall reaction) and about 50 (for a first-order wall

reaction), and the reaction order for loss of F is found to be 1.68. Kinetics analysis of the mass spectroscopy data shows that surface material is not a controlling factor for the generation of HF and F_2 under the conditions employed. The loss of F atoms shows kinetics results that indicate a reaction order (order = 1.68) that is consistent with a combination of surface and volume reactions. Production of F_2 has an overall order that is close to 2, suggesting that the generation of F_2 is mostly through a gas-phase reaction (pseudo-second order). Data for the production of HF show a surface-independent, relatively constant level of HF, which is consistent with a surface reaction (zero order or first order) for its generation. In the low-pressure region, pseudo-second-order assumptions break down, and the gas-phase reaction that generates F_2 looks more like a third-order reaction. To obtain a true reaction mechanism in this low-pressure regime (<0.5 Torr), a separate study is required that focuses specifically on this pressure range.

The decrease in the F atom concentration with increase in discharge pressure for the plasma flow is one of the main findings of this research. Of course, the main reason for this behavior is the pseudo-second-order reaction/recombination kinetics for the $F/F_2/HF$ system. The plasma conditions (electron energy, collision rates, NF_3 fragmentation, etc.) can also play a role in this behavior, but the details of the plasma dynamics are not known or well controlled for this system because the plasma impedance and coupling to the input radio frequency or microwave power are not constant.

Acknowledgment. We thank Colin Quinn (Advanced Energy Industries Inc.) for the low-frequency plasma source used in these studies and Eugene J. Karwacki (Air Products and Chemicals, Inc.) for the gas-handling equipment and NF_3.

References and Notes

(1) Yamaguchi, T.; Sasaki, K.; Kadota, K. *Plasma Chem. Plasma Process.* **2000**, *20*, 145.
(2) Kinoshita, K.; Noda, S.; Morishita, S.; Itabashi, N.; Okigawa, M.; Sekine, M.; Inoue, M. *J. Vac. Sci. Technol. A* **1999**, *17*, 1520 (Part 1).
(3) Matsuo, P. J.; Kastenmeier, B. E. E.; Oehrlein, G. S.; Langan, J. G. *J. Vac. Sci. Technol. A* **1999**, *17*, 2437.
(4) Kastenmeier, B. E. E.; Matsuo, P. J.; Oehrlein, G. S.; Langan, J. G. *J. Vac. Sci. Technol. A* **1998**, *16*, 2047.
(5) Tachibana, K.; Kamisugi, H.; Kawasaki, T. *Jpn. J. Appl. Phys. 1* **1999**, *38*, 4367.
(6) Booth, J. P. *Plasma Sources Sci. Technol.* **199**, *8*, 249.
(7) Fukasawa, T.; Nakamura, A.; Shindo, H.; Horiike, Y. *Jpn. J. Appl. Phys. 1* **1994**, *33*, 2139.
(8) Ishii, I.; Brandt, W. W. *J. Electrochem. Soc.* **1986**, *133*, 1240.
(9) Perrin, J.; Meot, J.; Siefert, J. M.; Schmitt, J. *Plasma Chem. Plasma Process.* **1990**, *10*, 571.
(10) Langan, J. G.; Rynders, S. W.; Felker, B. S.; Beck, S. E. *J. Vac. Sci. Technol. A* **1998**, *16*, 2108.
(11) Langan, J. G.; Beck, S. E.; Felker, B. S.; Rynders, S. W. *J. Appl. Phys.* **1996**, *79*, 3886 (Part 1).
(12) Larson, P. R.; Copeland, K. A.; Dharmasena, G.; Lasell, R. A.; Keil, M.; Johnson, M. B. *J. Vac. Sci. Technol. B* **2000**, *18*, 307.
(13) Pruette, L.; Karecki, S.; Reif, R.; Tousignant, L.; Reagan, W.; Kesari, S.; Zazzera, L. *J. Electrochem. Soc.* **2000**, *147*, 1149.
(14) Peters, A. M.; Nastasi, M. *J. Vac. Sci. Technol. A* **2001**, *19*, 2773.
(15) Hsueh, H. P.; McGrath, R. T.; Ji, B.; Felker, B. S.; Langan, J. G.; Karwacki, E. J. *J. Vac. Sci. Technol. B* **2001**, *19*, 1346.
(16) Reichardt, H.; Frenzel, A.; Schober, K. *Microelectron. Eng.* **2001**, *56*, 73.
(17) Novakovic, N. V.; Stojilkovic, S. M.; Milic, B. S.; Gajic, D. Z. *Czech J. Phys.* **2000**, *50*, 425.
(18) Sasaki, K.; Kawai, Y.; Kadota, K. *Rev. Sci. Instrum.* **1999**, *70*, 76 (Part 1).
(19) Sasaki, K.; Kawai, Y.; Suzuki, C.; Kadota, K. *J. Appl. Phys.* **1998**, *83*, 7482.
(20) Kawai, Y.; Sasaki, K.; Kadota, K. *Plasma Sources Sci. Technol.* **1998**, *7*, 36.
(21) Sasaki, K.; Kawai, Y.; Suzuki, C.; Kadota, K. *J. Appl. Phys.* **1997**, *82*, 5938.
(22) Kawai, Y.; Sasaki, K.; Kadota, K. *Jpn. J. Appl. Phys. 2* **1997**, *36*, L1261.
(23) Sasaki, K.; Kawai, Y.; Kadota, K. *Appl. Phys. Lett.* **1997**, *70*, 1375.
(24) Cunge, G.; Chabert, P.; Booth, J. P. *J. Appl. Phys.* **2001**, *89*, 7750.
(25) Shimizu, M.; Yasutake, K.; Ohmi, H.; Takeuchi, A.; Kakiuchi, H.; Yoshii, K.; Mori, Y. *Appl. Phys. B-Lasers Opt.* **2001**, *72*, 227.
(26) Tachibana, K.; Kamisugi, H. *Appl. Phys. Lett.* **1999**, *74*, 2390.
(27) Elyaakoubi, M.; Ranson, P. *J. Appl. Phys.* **1995**, *78*, 4733.
(28) Hansen, S. G.; Luckman, G.; Colson, S. D. *Appl. Phys. Lett.* **1988**, *53*, 1588.
(29) Schwarzenbach, W.; Tserepi, A.; Derouard, J.; Sadeghi, N. *Jpn. J. Appl. Phys. 1* **1997**, *36*, 4644.
(30) Tserepi, A.; Schwarzenbach, W.; Derouard, J.; Sadeghi, N. *J. Vac. Sci. Technol. A* **1997**, *15*, 3120.
(31) Raoux, S.; Tanaka, T.; Bhan, M.; Ponnekanti, H.; Seamons, M.; Deacon, T.; Xia, L. Q.; Pham, F.; Silvetti, D.; Cheung, D.; Fairbairn, K.; Johnson, A.; Pearce, R.; Langan, J. *J. Vac. Sci. Technol. B* **1999**, *17*, 477.
(32) Raoux, S.; Cheung, D.; Fodor, M.; Taylor, W. N.; Fairbairn, K. *Plasma Sources Sci. Technol.* **1997**, *6*, 405.
(33) Johnson, A. D.; Entley, W. R.; Maroulis, P. J. *Solid State Technol.* **2000**, *43*, 103.
(34) Oh, B. H.; Bae, J. W.; Kim, J. H.; Kim, K. J.; Ahn, Y. S.; Lee, N. E.; Yeom, G. Y.; Yoon, S. S.; Chae, S. K.; Ku, M. S.; Lee, S. G.; Cho, D. H. *Surf. Coat. Technol.* **2001**, *146*, 522.
(35) Tonnis, E. J.; Graves, D. B.; Vartanian, V. H.; Beu, L.; Lii, T.; Jewett, R. *J. Vac. Sci. Technol. A* **2000**, *18*, 393.
(36) Xu, X. D.; Rauf, S.; Kushner, M. J. *J. Vac. Sci. Technol. A* **2000**, *18*, 213.
(37) Jumper, E. J.; Wilkins, R. G.; Preppernau, B. L. *AIAA J.* **1988**, *26*, 57.
(38) Pavlenko, V. S.; Nalivaiko, S. E.; Egorov, V. G.; Gordon, E. B. *Kinet. Catal.* **1996**, *37*, 304.
(39) Meeks, E.; Larson, R. S.; Vosen, S. R.; Shon, J. W. *J. Electrochem. Soc.* **1997**, *144*, 357.
(40) Vosen, S. R.; Meeks, E.; Larson, R. S.; Shon, J. W. *J. Electrochem. Soc.* **1997**, *144*, 1514.
(41) Darcy, A.; Galijatovic, A.; Barth, R.; Kenny, T.; Krantzman, K. D.; Schoolcraft, T. A. *J. Mol. Graphics Model.* **1996**, *14*, 260.
(42) Wiley, W. C.; McLaren, I. H. *J. Mass Spectrom.* **1997**, *32*, 4.
(43) Wiley, W. C.; McLaren, I. H. *Rev. Sci. Instrum.* **1955**, *26*, 1150.
(44) Laidler, K. J. *Chemical Kinetics*; Harper & Row: New York, 1987.
(45) Steinfeld, J. I.; Francisco, J. S.; Hase, W. L. *Chemical Kinetics and Dynamics*; Prentice Hall: Upper Saddle River, NJ, 1999.
(46) Logan, S. R. *Fundamentals of Chemical Kinetics*; Longman: Essex, England, 1996.
(47) Vasiliev, A. A.; Bezmelnitsyn, V. N.; Sinianski, V. F.; Chaivanov, B. B. *J. Fluorine Chem.* **1999**, *95*, 153.
(48) Ultee, C. J. *Chem. Phys. Lett.* **1977**, *46*, 366.
(49) Singh, H.; Coburn, J. W.; Graves, D. B. *J. Vac. Sci. Technol. A* **2000**, *18*, 2680.
(50) Kota, G. P.; Coburn, J. W.; Graves, D. B. *J. Vac. Sci. Technol. A* **1999**, *17*, 282.
(51) Kota, G. P.; Coburn, J. W.; Graves, D. B. *J. Appl. Phys.* **1999**, *85*, 74.
(52) Manke, G. C.; Hager, G. D. *J. Phys. Chem. Ref. Data* **2001**, *30*, 713 and references therein.
(53) Nordine, P. C.; LeGrange, J. D. *AIAA J.* **1976**, *14*, 644.
(54) Guzov, I. P.; Kormer, S. B.; Lvov, L. V.; Punin, V. T.; Sinistyn, M. V.; Stankeev, E. A.; Urlin, V. D. *Kvantovaya Elektron. (Moscow)* **1976**, *3*, 2043.
(55) Valance, W.; Birang, B.; MacLean, D. I. Office of Naval Research Report No. FRK-116; 1971.
(56) Baulch, D. L.; Duxbury, J.; Grant, S. J.; Montague, D. C. *J. Phys. Chem. Ref. Data* **1981**, *10* (Suppl. No. 1), 721 pp.
(57) Lloyd, A. C. *Int. J. Chem. Kinet*. **1971**, *3*, 39.
(58) Benson, S. W.; Fueneo, T. *J. Chem. Phys.* **1962**, *36*, 1597.
(59) Shui, V. H.; Appleton, J. P.; Keck, J. C. *13th Symposium (International) on Combustion*; The Combustion Institute: Pittsburgh, PA, 1971.
(60) Ganguli, P. S.; Kaufman, M. *Chem. Phys. Lett.* **1974**, *25*, 221.